

Convection and Diffusion in Patterns in Oscillated Granular Media

**C. Bizon,¹ M. D. Shattuck,¹ John R. de Bruyn,^{1,2} J. B. Swift,¹
W. D. McCormick,¹ and Harry L. Swinney¹**

Received February 2, 1998

Motions of individual particles within the stripe and square patterns formed in oscillated granular media are studied using numerical simulations. Our event-driven molecular dynamics simulations yield standing wave patterns in good accord with those observed in experiments at the same frequency and acceleration amplitude. The patterns are subharmonic and so return to their initial macroscopic state after two external cycles. However, simulations reveal that individual particles do not return to their initial position. In addition to diffusive motion, an organized flow of particles within the patterns is found; associated with each peak and each valley of the pattern is a pair of counterrotating convection rolls. The diffusion is anisotropic: transport perpendicular to stripes is enhanced over that parallel to stripes. This enhancement is computed as a function of the layer depth, acceleration amplitude, frequency, and coefficient of restitution of the particles, and is attributed to the effect of the advective motion. Velocity distributions, granular temperature, and the dependence of the diffusion coefficient parallel to the stripes on the average granular temperature are studied.

KEY WORDS: Granular media; pattern; convection; enhanced diffusion; granular temperature; numerical simulation.

I. INTRODUCTION

Just as vertically oscillated fluids exhibit an instability to patterns of subharmonic standing waves,⁽¹⁻³⁾ so too do vertically oscillated granular media.⁽⁴⁻⁷⁾ Patterns observed in experiments on granular media include

¹ Center for Nonlinear Dynamics and Department of Physics, University of Texas, Austin, Texas 78712.

² Permanent address: Department of Physics and Physical Oceanography, Memorial University of Newfoundland, St. John's, Newfoundland, Canada.

stripes, squares, hexagons, and localized structures (oscillons). Direct simulations at the level of individual particles moving under Newton's laws have quantitatively reproduced many of these phenomena,^(8,9) but thousands of particle trajectories may represent an overabundance of detail. For many purposes a description in terms of a few averaged quantities may be more useful. Although there are situations in which continuum models will fail to describe the motion of granular assemblies,⁽¹⁰⁾ the similarity between the patterns formed by oscillated granular media and those formed in oscillated fluids, and the fluid-like motions seen in experiment⁽⁴⁻⁷⁾ and simulation^(8,9) suggest that a system of continuum equations may apply to this system.

The obvious starting point for a derivation of a continuum description is the kinetic theory of dense gases. Studies have proceeded along such lines for nearly two decades,⁽¹¹⁻¹⁴⁾ and have led to good agreement between theory and computer simulations in the case of simple shear flow;⁽¹⁵⁾ few other flows have been analyzed. The present work represents a preliminary step towards application of such ideas to oscillated granular patterns.

We examine in direct numerical simulations the self-diffusion of particles within the flow. Experimental measurements of the diffusion coefficient D would be difficult due to the problem of particle tracking within an opaque three-dimensional flow. It is in exactly such cases that numerical simulation can be most useful.

II. SIMULATION

We use an event driven code that has been successfully tested against experiment.⁽⁹⁾ In this simulation, particle collisions are instantaneous, conserve both linear and angular momentum, and dissipate energy. Between collisions, particles travel parabolically under the influence of gravity. Air friction is assumed to be negligible, as in experiments, which were conducted in evacuated containers.^(5,9)

When particles collide, new velocities and angular velocities are calculated for the particles using an instantaneous collision operator that depends upon three parameters: the linear coefficient of restitution e , the coefficient of friction μ , and the rotational coefficient of restitution, β .⁽¹⁶⁾ Experimentally, e is a function of collision velocity v_n . Further, simulations with a e that is independent of collision velocity are susceptible to divergences in the collision frequency.⁽¹⁷⁾ We let $e(v_n) = 1 - Bv_n^\alpha$ for v_n less than a crossover velocity v_0 , and $e(v_n) = \varepsilon$ for $v_n > v_0$, where $B = (1 - \varepsilon)(v_0)^{-\alpha}$, $\alpha = 0.75$, $v_0 = \sqrt{g\sigma}$, σ is the particle diameter, g is the gravitational acceleration, and ε is a constant. Simulations with $\varepsilon = 0.7$, $\mu = 0.5$, and

$\beta = 0.35$ correctly reproduce the patterns and their wavelengths obtained from experiments with lead and bronze spheres over a wide range of control parameters,⁽⁹⁾ so we adopt these values for the present study.

We simulate particles in an oscillating box with periodic boundary conditions in both horizontal directions. The floor of the box oscillates vertically with $z_{\text{floor}} = A \sin 2\pi ft$, where A is the amplitude, f the frequency of vibration, and t is time. The nondimensional control parameters are the acceleration amplitude $\Gamma = A(2\pi f)^2/g$, the frequency $f^* = f \sqrt{H/g}$, and the layer depth $N = H/\sigma$, where H is the physical depth of the layer. This nondimensionalization has the advantage of collapsing much of the wavelength vs. frequency data onto a single curve.⁽¹⁸⁾ Patterns form when Γ exceeds a critical threshold $\Gamma_c \approx 2.5$. The pattern that forms when Γ exceeds Γ_c is squares for f^* less than about 0.35 and stripes for higher f^* .

III. CONVECTION

Gross features of the particle flow within patterns have been described by several authors.^(8, 19) For patterned states, $\Gamma > 1$, so that the layer of particles leaves the floor of the box during each oscillation. When the layer collides with the floor, peaks collapse and particles under the collapsing peaks are pushed away horizontally. Approximately one half of a cycle later, the layer is nearly flat, but large horizontal and vertical velocities within the layer cause new peaks to grow, offset by one half of a wavelength from their previous positions. Particles collide with the container floor again after a further oscillation, and one period later (after a total of two vibration periods) the pattern has returned to its initial state.

A naive view of particle motions in the layer would assume two processes: the sloshing motion that transports large numbers of particles one half of a wavelength each period, and diffusion. The diffusive motion could be isolated by examining the positions of the particles every two periods. Since the macroscopic pattern itself has returned to its initial state, observed particle displacements would be due to diffusion.

This simple view, however, is incorrect. In addition to the sloshing motion and diffusion, simulations with 60000 particles in a square box of side length 100σ show an additional convective motion within the flow, as Fig. 1 illustrates. This motion was observed by calculating particle displacements over two periods. If these displacements were due to diffusion, then time and spatial averages of the displacement field would give zero; they do not. We average the displacement field in one spatial direction—along a stripe for a striped pattern, or across the width of a peak for a square pattern. Treating this averaged displacement field as a velocity field, we numerically calculate streamlines, using particle positions as initial

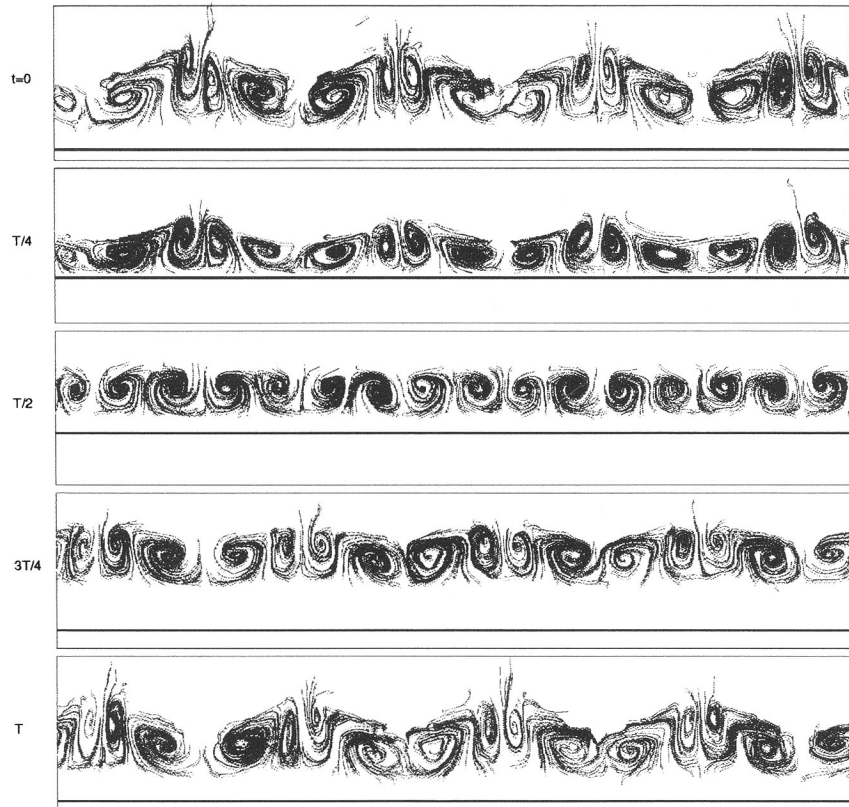


Fig. 1. Side view of convection rolls in granular patterns at $\Gamma = 3.0$, $f^* = 0.35$, and $N = 5.4$. The standing wave pattern is stripes pointing into the page. Streamlines are colored with the sign of the vorticity; clockwise rotations are green, counterclockwise are red. The solid horizontal line in each frame is the bottom of the container.

conditions. The results of 500 such integrations, for displacement fields calculated at several phases of the cycle, are displayed in Fig. 1.

The resulting streamlines reveal a series of convection rolls. Four rolls are associated with each wavelength of the pattern, so that particles descend at the centers of peaks and valleys, and ascend in between. The rolls persist throughout the cycle, contracting and expanding with the sloshing motion, but keeping the positions of the downflows fixed. As the frequency of oscillation increases, the wavelength of the pattern decreases compared to the depth of the layer, but the number of convection rolls per wavelength stays the same. Therefore, at higher frequencies the rolls are thin, while at lower frequencies, they are wide, as shown in Fig. 2. The rolls

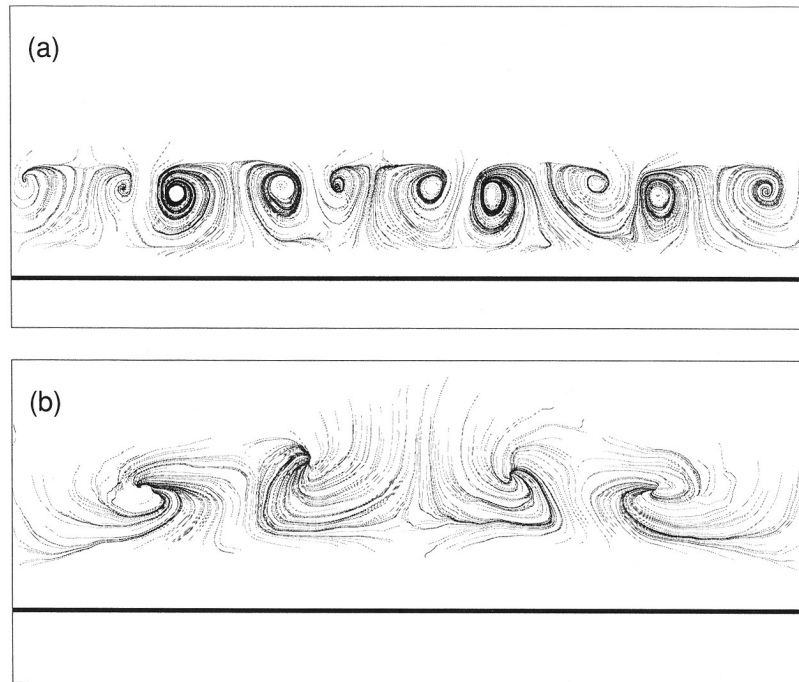


Fig. 2. As frequency increases, pattern wavelength decreases, changing the aspect ratio of the convection rolls. At (a) $f^* = 0.464$, the pattern is stripes and at (b) $f^* = 0.27$, squares. Each picture displays one half of the lateral extent of the cell, and both patterns are obtained for $\Gamma = 3.0$. For each frequency, the layer is at its maximum height.

exist for both stripe and square patterns. In stripe patterns the rolls lie parallel to the stripes, while in square patterns the convection forms cellular structures with the symmetry of the pattern; see Fig. 3.

Experiments in oscillated granular materials without patterns have also shown convection.⁽²⁰⁾ Typically, grains move down along the walls of the container and up in its center, sometimes forming a heap. The two mechanisms proposed for such behavior, forcing by air⁽²¹⁾ and by friction at the lateral walls,⁽²²⁾ cannot be responsible for the convection we observe, since our simulation includes neither the air flow nor lateral walls. The rolls appear to be driven by the standing wave pattern itself; hence their spatial slaving to the pattern. When the layer collides with the plate, pressure increases under the peaks, forcing particles to move horizontally. The maximum horizontal pressure gradient is not at the bottom of the layer, since particles in the valley resist motion, but at the base of the peak, where particles are free to move horizontally over those in the valley. Particles at the

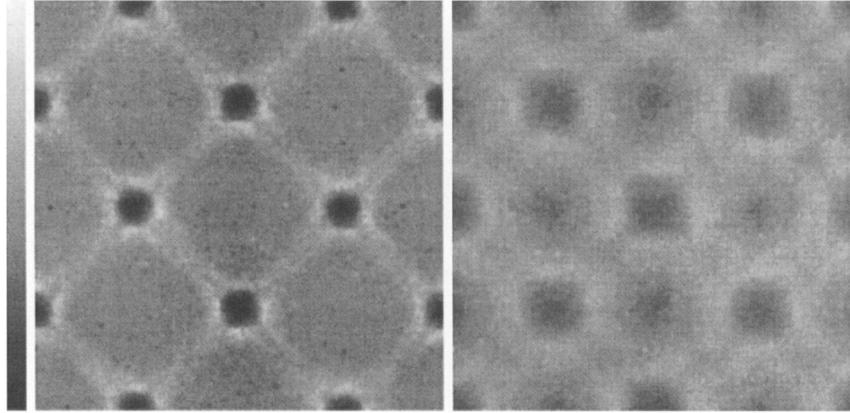


Fig. 3. Overhead view of convection rolls for a square pattern at $f^* = 0.27$, $\Gamma = 3.0$, and $N = 5.4$. The grayscale indicates the vertical displacement of particles over two driving cycles, with white indicating upward motion and black downward motion. In the left image, the peaks are near their full height and are centered over the strong downflows, while the right image shows the layer near its flattest point.

base of the peaks acquire the largest horizontal velocities, and the location from which these particles begin to move when the layer strikes the plate is coincident with the upflow of the rolls.

IV. DIFFUSION

In fluids, advection can lead to enhanced diffusion. Dye injected into a Rayleigh–Bénard convection cell travels more rapidly perpendicular to the rolls than it does parallel to the rolls.⁽²³⁾ On scales large compared to the roll size, the perpendicular motion appears diffusive, but with a diffusion coefficient larger than the molecular value. With both sloshing and convection operating within the granular medium, it seems likely that enhanced diffusion will occur in this system as well.

To study diffusion, we conduct simulations in a doubly periodic cell with horizontal dimensions L_x and L_y , such that $L_x \ll L_y$. With this geometry, stripes unambiguously form parallel to L_x . In analogy with the experiments on convection, we treat all motion as diffusive. To compute the effective diffusion coefficients, we record the positions of the particles at intervals of two periods, i.e., each time the pattern returns to a particular macroscopic state. During this interval, each particle moves a horizontal distance l_{\perp} perpendicular to the stripes and l_{\parallel} parallel to them. Treating diffusion in each direction as a one-dimensional random walk with a temporal step size of $2/f$, the diffusion coefficient D is determined from the

mean square jump length by $D_{\parallel} = \langle l_{\parallel}^2 \rangle f/4$ and $D_{\perp} = \langle l_{\perp}^2 \rangle f/4$. In order to collect statistics for the jump lengths, simulations are allowed to run for at least 100 oscillations, once a steady pattern is reached. In contrast to the experiments on Rayleigh–Bénard convection, our calculation does not correspond to a time scale large compared to the diffusion time across a pattern wavelength. Rather than computing diffusion across many rolls, we compute diffusion within one wavelength of the pattern.

In studies of the pattern wavelength as a function of frequency, it was found that the wavelength of the pattern depended on N , the nondimensional depth of the layer.^(5, 7) However, if the wavelength and frequency are scaled with H and $\sqrt{g/H}$ respectively, many of the data collapse, effectively removing N as a control parameter.⁽¹⁸⁾ To determine whether the diffusion coefficient displays the same behavior, we performed simulations at $f^* = 0.464$ and $\Gamma = 3$ for four layer depths, N , between 3.6 and 10.8. In each case, $L_x/\sigma = 10.5$ and $L_y/H = 18.5$. Since the wavelength scales with H at fixed f^* , scaling L_y in the same manner produces the same number of stripes in each run.

Figure 4(a) shows the nondimensional diffusion coefficients $D^* = D/\sqrt{H^3g}$ parallel to and perpendicular to the stripes; the ratio $D_{\perp}^*/D_{\parallel}^*$ is displayed in Fig. 4(b). In all cases, $D_{\perp}^* > D_{\parallel}^*$, showing enhanced diffusion perpendicular to the stripes. As the depth decreases, so does the difference

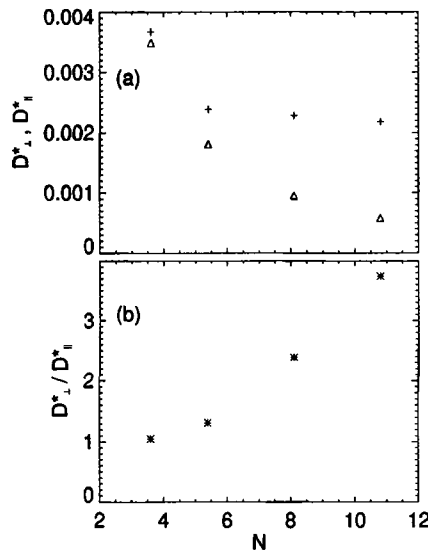


Fig. 4. (a) Nondimensional diffusion coefficients perpendicular to stripes (+) and parallel to stripes (Δ) and (b) diffusion coefficient ratio, as a function of $N = H/\sigma$. For $N < 3.6$, the patterns do not form at these parameter values ($\Gamma = 3.0$, $f^* = 0.46$).

in the two coefficients. The smallest N which appears on the graph is the smallest for which patterns form. With the exception of this point, we note that D_{\perp}^* varies only slowly with N , although the same is not true of D_{\parallel}^* . Thus, scaling with H does not completely remove N as a control parameter. The different behavior of the two diffusion coefficients suggests that they are being controlled by different processes. Specifically, the fact that both the wavelength and the perpendicular diffusion coefficient scale with H suggests that perpendicular diffusion is controlled by the flow of the particles within the pattern.

To investigate the dependence of the diffusion coefficient on f^* and Γ , we perform simulations of 6316 particles in a box, periodic in both horizontal directions, and with $L_x = 10.5\sigma$ and $L_y = 100\sigma$, so that $N = 5.4$, the shallowest layer for which a D_{\perp}^* nearly constant with N is reached. This reduces the amount of computational time required to produce many oscillations.

Figure 5(a) displays the computed dimensionless diffusion coefficients in each direction as a function of f^* at $\Gamma = 3.0$; the ratio of perpendicular to parallel diffusion coefficients is displayed in Fig. 5(b). For all frequencies, diffusion perpendicular to the stripes is enhanced in comparison to that parallel to the stripes. At high frequencies, where the pattern amplitude

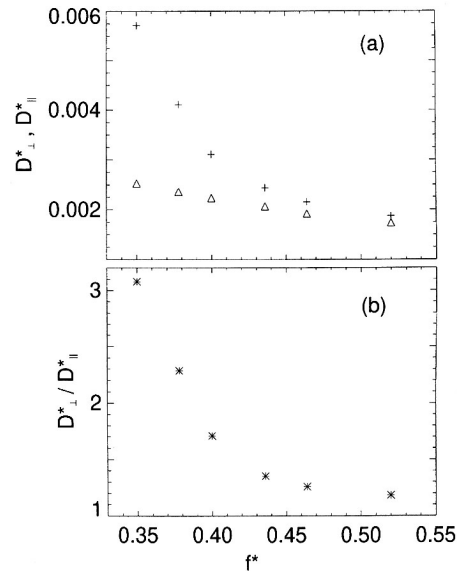


Fig. 5. (a) Nondimensional diffusion coefficients perpendicular to stripes (+) and parallel to stripes (Δ) and (b) diffusion coefficient ratio, as a function of f^* . For $f^* < 0.35$, patterns undergo a transition to squares. For these runs, $\Gamma = 3.0$, $N = 5.4$.

is small, diffusion proceeds in both directions at nearly equal rates. As the frequency decreases, the pattern amplitude increases, as do both diffusion coefficients. The perpendicular diffusion, however, grows at a much faster rate, so that the ratio D_{\perp}/D_{\parallel} grows to 3.1 at $f^* = 0.35$.

Figure 6 displays the diffusion coefficients and their ratio as a function of Γ , with fixed $f^* = 0.35$. For this frequency and depth, the transition from a flat layer to a patterned state occurs for Γ between 2.5625 and 2.59375, i.e., patterns are stable at the higher Γ , but not at the lower. Below onset, the diffusion is nearly isotropic (in this case perpendicular and parallel directions are in reference to the short side of the box); when patterns form, the diffusion becomes strongly anisotropic due to a large increase in diffusion perpendicular to the stripes. We compare the amount of anisotropy $D_{\perp}^*/D_{\parallel}^* - 1$ to the distance above onset $\Gamma - \Gamma_c$ in Fig. 7. For this figure, we set $\Gamma_c = 2.578125$, halfway between the values that bound the onset. The anisotropy scales with the distance above onset over nearly two decades.

In addition to variation of the external control parameters, we study the effect of varying ε , the coefficient of restitution of the model particle. Note that ε , however, is not identical to the coefficient of restitution of the real particle being modeled. While the restitution coefficient in both simulation and experiment control the amount of energy dissipated in collisions,

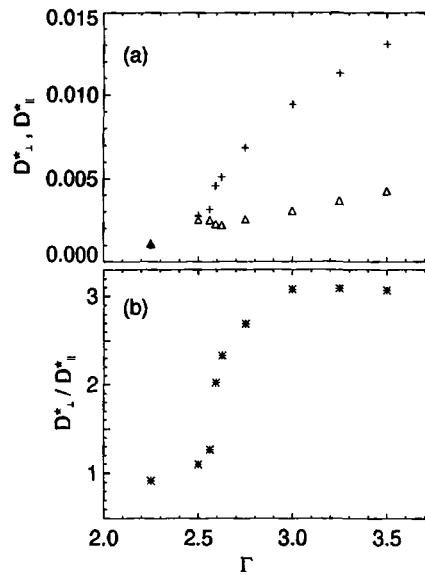


Fig. 6. (a) Nondimensional diffusion coefficients perpendicular to stripes (+) and parallel to stripes (Δ) and (b) their ratio, as a function of Γ . Onset of patterns occurs between $\Gamma = 2.5625$ and $\Gamma = 2.59375$. For these data $N = 5.4$ and $f^* = 0.35$.

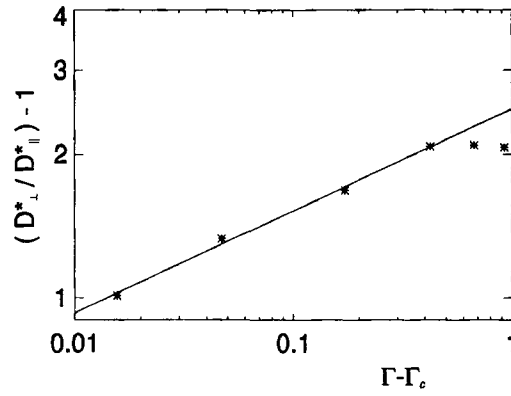


Fig. 7. Diffusion anisotropy as a function of distance above onset. The best fit line has slope 0.21 ± 0.05 , where the uncertainty is determined by allowing Γ_c to vary between the two bounding Γ 's. The parameters are those given in Fig. 6.

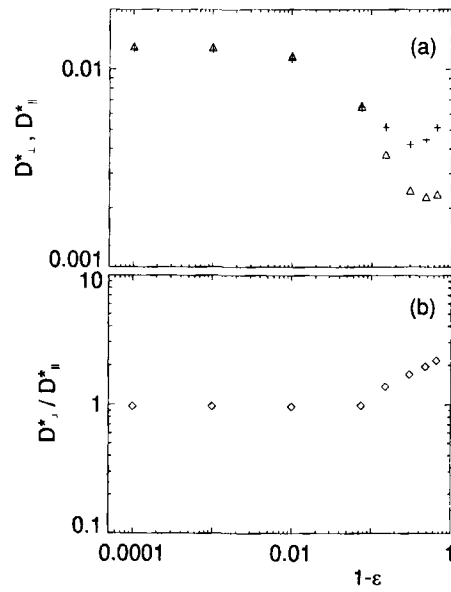


Fig. 8. (a) Nondimensional diffusion coefficients perpendicular to stripes (+) and parallel to stripes (Δ) and (b) their ratio, as a function of $1 - \epsilon$. Patterns exist for $\epsilon \leq 0.925$. For these data, $\Gamma = 3.0$, $f^* = 0.4$, $N = 5.4$.

the infinitesimally short collision durations of the model forces deviation from the physical value. Because real collisions have a finite duration, a real layer of particles colliding with an oscillating plate undergoes fewer dissipative collisions than the event driven code simulates. In order to model correctly the total dissipation in the layer, each model collision must be less dissipative than its physical counterpart; hence the values of ε used in the simulations are greater than the physical value.

Variation of ε varies the dissipation of energy within the layer. We compute the diffusion coefficients as ε varies from 0.35, corresponding to very dissipative particles, to 0.9999, corresponding to nearly elastic particles. However, since we have not varied the friction coefficient μ , enough energy is dissipated in collisions for the layer to remain in its compact state. The results are summarized in Fig. 8. For $\varepsilon > 0.925$, the layer no longer supports patterns, and the diffusion is isotropic. As ε decreases, the layer becomes more dense, allowing patterns to form. Fitting a line through the points for which a pattern exists on Fig. 8(b), we find that $D_{\perp}^*/D_{\parallel}^* - 1 \propto (1 - \varepsilon)^{0.77 \pm 0.05}$. For the lowest ε , both diffusion coefficients again increase, but there is no noticeable change in behavior of the ratio of the coefficients.

V. VELOCITY DISTRIBUTIONS AND TEMPERATURE DEPENDENCE

While D_{\perp}^* is controlled by the advective motion of particles within the pattern, diffusion parallel to stripes or in the absence of patterns is presumably governed by the bulk properties of the layer. That is, we suppose that D_{\parallel}^* is a function of the thermodynamic state of the layer, which is in turn set by the external control parameters and the properties of the particles.

With this motivation and with the idea of obtaining a result that may be useful in testing granular kinetic theory, we examine the dependence of D_{\parallel}^* on the granular temperature. Granular temperature, defined in analogy to thermodynamic temperature, is related to the mean square velocity fluctuation by⁽²⁶⁻²⁸⁾

$$kT_i = m \langle (v_i - \langle v_i \rangle)^2 \rangle \quad (1)$$

where m is the mass of a particle, k is a constant analogous to Boltzmann's constant and relates the fluctuation energy to a temperature scale, i indicates the component of the velocity in question (either \parallel or \perp), and the angle brackets denote an ensemble average at a particular spatial point and phase in the cycle. In general, T will be a function of position and time, and could be anisotropic.

Since $D_{||}^*$ is computed over all particles regardless of their location within the flow, and because we assume that at all locations and times the average velocity parallel to the stripes is zero, we calculate the average in Eq. (1) over all particles. Figure 9(a) displays the nondimensional mean square velocity parallel to the stripes as a function of phase of the cycle. Velocity distributions at three phases near the collision are displayed in

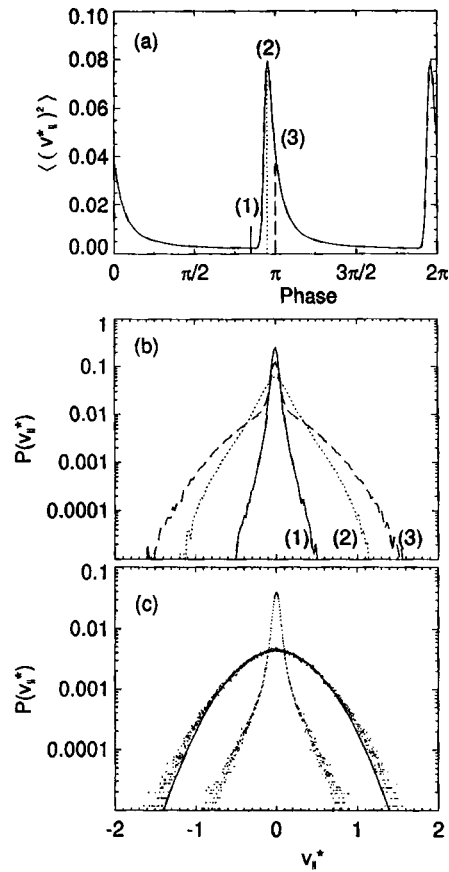


Fig. 9. (a) Mean square velocity parallel to stripes as a function of phase for $\Gamma = 3.0$, $f^* = 0.436$, $N = 5.4$. The peak occurs when the layer collides with the plate. (b) Velocity distribution functions for the phases indicated in (a). (c) Velocity distribution functions of two populations of particles at phase (2). Particles that have interacted with the plate have a nearly gaussian distribution (the solid curve is a gaussian fit). The remaining particles have a narrower distribution similar to the velocity distribution function before the collision. The particles in the broader distribution are those which have vertical position less than 4σ above the plate and vertical velocity greater than $-0.9\sqrt{gH}$.

Fig. 9(b). The distribution is at its narrowest just before the collision. When the layer collides with the plate, the layer is violently heated. Initially, only the particles closest to the plate are heated, so that the layer may be considered as two populations of particles: particles near the bottom of the layer that have been heated by the layer and particles at the top of the layer that have not yet interacted with the plate via the particles beneath them. In the phase space of vertical position vs. vertical velocity, these populations are relatively distinct, and velocity distribution functions may be constructed separately for each population, as shown in Fig. 9(c). The lower particles have the broader distribution. In addition to increasing their velocity, the many particle collisions drive the distribution towards a Maxwell-Boltzmann distribution. The distribution function for the higher particles is similar to that of the entire layer just prior to the collision. As the layer is lifted by the plate, the upper reaches of the layer are excited, but because of the inelastic nature of the collisions, the layer again begins to cool, narrowing the distribution until the following collision.

Averaging Eq. (1) over phase, as indicated by the overline, we have $\overline{\langle v_{\parallel}^2 \rangle} = k\overline{T_{\parallel}}/m$, or nondimensionalizing,

$$\tau^* \equiv k\overline{T_{\parallel}}/mgH = \overline{\langle v_{\parallel}^2 \rangle}/gH \quad (2)$$

where τ^* is a single parameter that describes the thermal activity for a particular set of control parameters and particle properties.

In Fig. 10 we plot D_{\parallel}^* as a function of τ^* for the data with different values of ε , that is, the data in Fig. 8. The plot of D_{\parallel}^* is nearly linear with τ^* for data points which both do and do not correspond to patterned states. Given this somewhat surprising success of finding a single thermodynamic quantity that determines D_{\parallel}^* , we attempt to unify the previous results. In Fig. 11 we plot the values of D_{\parallel}^* obtained from the simulations discussed above, as well as a second set obtained from variation in Γ , and a number of other simulations, as summarized in Table I. While the level of collapse is reasonable, several of the data points do not lie on the common curve; D_{\parallel}^* is not simply a function of τ^* . However, we find empirically that all of our results for D_{\parallel}^* as a function of Γ , f^* , N , and ε can be described as a function of a single scaled temperature,

$$D_{\parallel}^* = F\left(\frac{\tau^*\Gamma}{f^*N^{1/2}}\right) \quad (3)$$

as shown in Fig. 12.

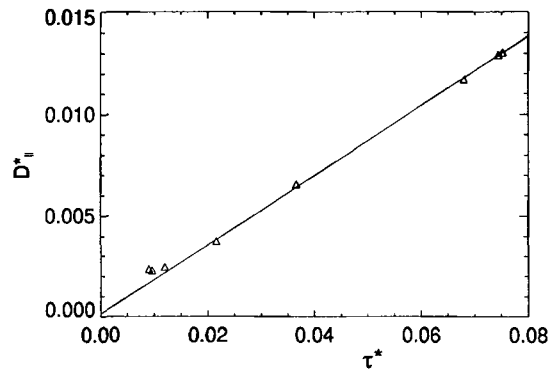


Fig. 10. Diffusion coefficient parallel to stripes versus nondimensional average granular temperature for the data plotted in Fig. 8. The line is a best fit to the data for which $\tau^* > 0.2$.

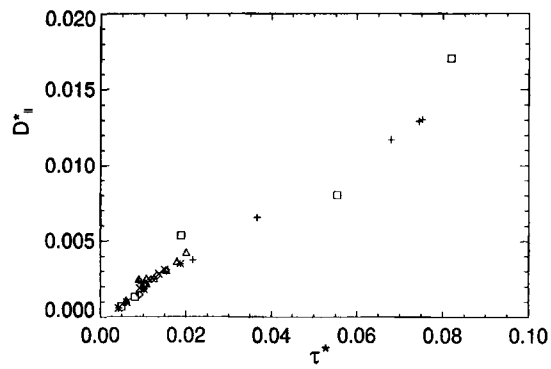


Fig. 11. Diffusion coefficient parallel to stripes versus average temperature for the data in Table I.

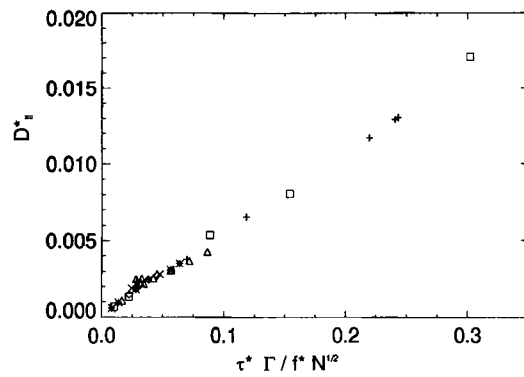


Fig. 12. Diffusion coefficient parallel to stripes versus rescaled average temperature for the data in Table I.

Table I. Simulation Parameters

Γ	f^*	N	ε	symbol
3.0	0.35	5.4	0.7	◇
3.0	0.378	5.4	0.7	◇
3.0	0.4	5.4	0.7	◇
3.0	0.436	5.4	0.7	◇
3.0	0.464	5.4	0.7	◇
3.0	0.52	5.4	0.7	◇
2.25	0.35	5.4	0.7	△
2.5	0.35	5.4	0.7	△
2.5625	0.35	5.4	0.7	△
2.59375	0.35	5.4	0.7	△
2.625	0.35	5.4	0.7	△
2.75	0.35	5.4	0.7	△
3.0	0.35	5.4	0.7	△
3.25	0.35	5.4	0.7	△
3.5	0.35	5.4	0.7	△
3.25	0.4	5.4	0.7	×
3.5	0.4	5.4	0.7	×
2.5	0.4	5.4	0.7	×
2.75	0.4	5.4	0.7	×
3.0	0.464	3.6	0.7	*
3.0	0.464	5.4	0.7	*
3.0	0.464	8.1	0.7	*
3.0	0.464	10.8	0.7	*
3.0	0.4	5.4	0.35	+
3.0	0.4	5.4	0.535	+
3.0	0.4	5.4	0.7	+
3.0	0.4	5.4	0.85	+
3.0	0.4	5.4	0.925	+
3.0	0.4	5.4	0.99	+
3.0	0.4	5.4	0.999	+
3.0	0.4	5.4	0.9999	+
3.0	0.378	8.1	0.7	□
3.0	0.43	10.8	0.7	□
3.0	0.464	5.4	0.99	□
3.0	0.35	5.4	0.99	□
3.0	0.387	3.735	0.5	□

VI. DISCUSSION

We have explored the dynamics of particles within patterns in granular media. We have found that the motions of these particles may be decomposed into three processes. First, particles slosh back and forth forming subharmonic standing waves in the layer. Second, superimposed on this motion is a set of convection rolls: when the pattern returns to its initial position, the particles that compose it have moved in an organized way. Third, particles diffuse within the flow. When stripe patterns are present, the flow of particles perpendicular to the stripes controls the diffusion in that direction, leading to an enhancement over the diffusion parallel to stripes. This enhancement grows with the strength of patterns, increasing as Γ increases, f^* decreases, and ε decreases. We find that the diffusion coefficient parallel to the stripes depends on a single variable, the average granular temperature rescaled with the control parameters.

Note again that Eq. (3) is completely empirical; further, it is constructed from a set of data points that, while representing a large amount of computational time, are somewhat sparse in the $(\Gamma, f^*, N, \varepsilon)$ parameter space. Nevertheless, the relation can perhaps provide a useful starting point for modelers of oscillated granular media, especially if the proportionality between self-diffusion and viscosity from the kinetic theory of elastic particles holds in the oscillated granular system.

The diffusion coefficients that we have presented are all dimensionless. Nondimensional diffusion coefficients on the order of 5×10^{-3} translate into dimensional diffusion coefficients of about $5 \times 10^{-3} \text{ cm}^2 \text{ s}^{-1}$, assuming a typical layer depth of $H = 0.1 \text{ cm}$. Given that the pattern wavelength in such layers is 0.5 cm at 30 Hz , we calculate a diffusion time across a wavelength to be 50 seconds, or 1500 oscillations. An experimental cell of 10 cm diameter will have a horizontal diffusion time parallel to the stripes of five and a half hours.

ACKNOWLEDGMENTS

We thank Michael Marder for helpful discussions. This research is supported by the Department of Energy Office of Basic Energy Sciences and the Texas Advanced Research Program.

REFERENCES

1. S. Douady, *J. Fluid Mech.* **221**:383 (1990).
2. S. Fauve, K. Kumar, and C. Laroche, *Phys. Rev. Lett.* **68**:3160 (1992).
3. W. S. Edwards and S. Fauve, *J. Fluid Mech.* **278**:123 (1994).

4. F. Melo, P. Umbanhowar, and H. L. Swinney, *Phys. Rev. Lett.* **72**:172 (1994).
5. F. Melo, P. B. Umbanhowar, and H. L. Swinney, *Phys. Rev. Lett.* **75**:3838 (1995).
6. P. Umbanhowar, F. Melo, and H. L. Swinney, *Nature* **382**:793 (1996).
7. E. Clément, L. Vanel, J. Rajchenbach, and J. Duran, *Phys. Rev. E* **53**:2972 (1996).
8. S. Luding, E. Clément, J. Rajchenbach, and J. Duran, *Europhys. Lett.* **36**:247 (1996).
9. C. Bizon, M. D. Shattuck, J. B. Swift, W. D. McCormick, and H. L. Swinney, *Phys. Rev. Lett.* **80**:57 (1998).
10. Y. Du, H. Li, and L. P. Kadanoff, *Phys. Rev. Lett.* **74**:1268 (1995).
11. J. T. Jenkins and S. B. Savage, *J. Fluid Mech.* **130**:187 (1983).
12. C. K. K. Lun, S. B. Savage, D. J. Jeffrey, and N. Chepurmy, *J. Fluid Mech.* **140**:223 (1983).
13. J. T. Jenkins and M. W. Richman, *Arch. Rat. Mech. Anal.* **87**:355 (1985).
14. N. Sela, I. Goldhirsch, and S. H. Noskowitz, *Phys. Fluids* **8**:2337 (1996).
15. C. S. Campbell, *Annu. Rev. Fluid Mech.* **2**:57 (1990).
16. O. R. Walton, in *Particulate Two-Phase Flow*, M. C. Roco, ed. (Butterworth-Heinemann, Boston, 1993), pp. 884–911.
17. S. McNamara and W. R. Young, *Phys. Fluids A* **4**:496 (1992).
18. P. B. Umbanhowar, F. Melo, and H. L. Swinney, to be published.
19. K. M. Aoki and T. Akiyama, *Phys. Rev. Lett.* **77**:4166 (1996); C. Bizon, M. D. Shattuck, P. B. Umbanhowar, J. T. Newman, J. B. Swift, W. D. McCormick, and Harry L. Swinney, *ibid.* **79**:4713 (1997); K. M. Aoki and T. Akiyama, *ibid.* **79**:4714 (1997).
20. H. M. Jaeger, S. R. Nagel, and R. P. Behringer, *Physics Today* **49**:32 (1996).
21. H. K. Pak, E. Van Doorn, and R. P. Behringer, *Phys. Rev. Lett.* **74**:4643 (1995).
22. E. E. Ehrichs, H. M. Jaeger, G. S. Karczmar, J. B. Knight, V. Yu. Kuperman, and S. R. Nagel, *Science* **267**:1632 (1995).
23. T. H. Solomon and J. P. Gollub, *Phys. Fluids* **31**:1372 (1988).
24. M. N. Rosenbluth, H. L. Berk, I. Doxas, and W. Horton, *Phys. Fluids* **30**:2636 (1987).
25. B. I. Shraiman, *Phys. Rev. A* **36**:261 (1987).
26. J. T. Jenkins and M. W. Richman, *J. Fluid Mech.* **192**:313 (1988).
27. M. W. Richman, *J. Rheology* **33**:1293 (1989).
28. G. D. Cody, D. J. Goldfarb, G. V. Storch, Jr., A. N. Norris, *Powder Tech.* **87**:211 (1996).